Reaction4Exp example for inelastic scattering: the ^{64}Zn(^{16}O,^{16}O)^{64}Zn*(2^+) reaction

Introduction

This document describes briefly the use of the Reaction4Exp website for the case of inelastic scattering. We will use as example the ^{16}O+^{64}Zn $\rightarrow$ ^{16}O+^{64}Zn(2^+) reaction. This physics case is taken from the reference of Tenreiro *et al*, Physical Review C53, p. 2870 (1996), Ref. I hereafter.

The link to the elastic scattering website is:

https://reaction4exp.us.es/elastic/index.php

1 Reminder of the DWBA approximation

To describe an inelastic process of the form $a + A \rightarrow a + A^*$ (target excitation) within the DWBA approximation the projectile–target interaction is conveniently written as:

$$V(\mathbf{R}, \xi) = V_0(R) + \Delta V(\mathbf{R}, \xi), \tag{1}$$

where $V_0(R)$ contains in general nuclear and Coulomb parts, and describes the relative motion of the projectile and target, and $\Delta(\mathbf{R}, \xi)$ is the part of the projectile–target interaction which is responsible for the inelastic process. It depends on the internal coordinates of the nucleus being excited ($\{\xi\}$) as well as on the projectile–target relative coordinate ($\mathbf{R}$).

We consider that the target nucleus is initially in its ground state, described by some wavefunction $\phi_i(\xi)$, and is excited to some state $\phi_f(\xi)$. Within the DWBA approximation, the scattering amplitude for this process is given by:

$$\boxed{f_{fi}(\theta) = -\frac{\mu}{2\pi\hbar^2} \int d\mathbf{R}\ \chi_f^{(-)*}(\mathbf{K}_f, \mathbf{R}) \Delta V_{if}(\mathbf{R}) \chi_i^{(+)}(\mathbf{K}_i, \mathbf{R}),} \tag{2}$$

where θ is the scattering angle (in c.m. frame) and $\Delta V_{if}(\mathbf{R})$ is the *transition potential*

$$\boxed{\Delta V_{if}(\mathbf{R}) = \int d\xi \phi_f^*(\xi) \Delta V(\xi, \mathbf{R}) \phi_i(\xi).} \tag{3}$$

In Eq. (2), $\chi_i^{(+)}(\mathbf{K}_i, \mathbf{R})$ is the distorted-wave describing the projectile-target relative motion in the incident channel. This distorted-wave is the solution of the Schrödinger equation with the average potential $V_0(R)$:

$$\left[-\frac{\hbar^2}{2\mu_{aA}} \nabla^2_{\mathbf{R}} + V_0(R) - E_i \right] \chi_i^{(+)}(\mathbf{K}_i, \mathbf{R}) = 0 \tag{4}$$

where E_i is the c.m. kinetic energy in the entrance channel. Typically, the nuclear part of the optical potential $V_0(R)$ is parametrized in terms of some convenient form (e.g. Woods-Saxon shape) and the parameters adjusted to reproduce the elastic angular distribution. Analogously, $\chi_f^{(-)}(\mathbf{K}_i, \mathbf{R})$ is the corresponding distorted wave for the final channel. In practice, we use the same potential as for the incident channel.

2 Radial formfactors in the collective model

In many practical situations, such as in the collective models considered here, it is possible to write:

$$\Delta V(\mathbf{R},\xi) = \sum_{\lambda>0} \mathcal{F}_\lambda(R) \sum_\mu \mathcal{T}_{\lambda,\mu}(\xi) Y_{\lambda\mu}(\hat{R}) \tag{5}$$

The transition potential is given by:

$$\Delta V_{if}(\mathbf{R}) \equiv \langle I_f M_f | \Delta V(\mathbf{R},\xi) | I_i M_i \rangle = \sum_{\lambda>0} \mathcal{F}_\lambda(R) \langle I_f M_f | \mathcal{T}_{\lambda\mu}(\xi) | I_i M_i \rangle Y_{\lambda\mu}(\hat{R}) \tag{6}$$

where the *formfactor* $\mathcal{F}_\lambda(R)$ contains the radial dependence and $\mathcal{T}_{\lambda\mu}$ is a given multipole operator depending on the structure model. Using the Wigner-Eckart theorem:

$$\langle I_f M_f | \mathcal{T}_{\lambda\mu}(\xi) | I_i M_i \rangle = (2I_f+1)^{-1/2} \langle I_f M_f | I_i M_i \lambda\mu \rangle \langle I_f \| \mathcal{T}_\lambda(\xi) \| I_i \rangle_{\rm BM} \tag{7}$$

where $\langle I_f \| \mathcal{T}_\lambda(\xi) \| I_i \rangle$ are the so-called reduced matrix elements.

We consider two important cases:

2.1 Coulomb excitations

The coupling potentials are given by:

$$\Delta V_{if}(\mathbf{R}) \equiv \langle f; I_f M_f | \Delta V | i; I_i M_i \rangle = \sum_{\lambda>0,\mu} \frac{4\pi\kappa}{2\lambda+1} \frac{Z_t e}{R^{\lambda+1}} \langle f; I_f M_f | \mathcal{M}(E\lambda,\mu) | i; I_i M_i \rangle Y_{\lambda\mu}(\hat{R}) \tag{8}$$

where we see that $\mathcal{T}_{\lambda,\mu} \to \mathcal{M}(E\lambda,\mu)$ is the electric multipole operator. Its reduced matrix elements are related to the electric transition probability

$$B(E\lambda; i \to f) = \frac{1}{2I_i+1} |\langle f; I_f || \mathcal{M}(E\lambda) || i; I_i \rangle|^2. \tag{9}$$

In the collective rotor model, the $B(E\lambda)$ value can be related to the so-called **intrinsic reduced matrix element** ($Mn(E\lambda)$):

$$\sqrt{B(E\lambda; I_i \to I_f)} = i^{I_i - I_f + |I_i - I_f|} \langle I_i K \lambda 0 | I_f K \rangle Mn(E\lambda) \tag{10}$$

where K is the bandhead for the rotational band (for low-lying states of even-even nuclei K is usually 0). If the initial state has spin $I_i = 0$, then $Mn(E\lambda) = \pm\sqrt{B(E\lambda; 0 \to I_f)}$.

2.2 Nuclear excitations

For small nuclear deformations the projectile-target nuclear interaction can be expanded as:

$$V(\mathbf{R},\xi) \simeq V(R-R_0) - \sum_{\lambda,\mu} \hat{\delta}_{\lambda\mu} \frac{dV(R-R_0)}{dR} Y_{\lambda\mu}(\theta,\phi) + \ldots \tag{11}$$

where $\hat{\delta}_\lambda$ are deformation length operators. Hence, the transition potentials for nuclear excitations (with $\lambda > 0$) are

$$V_{if}(\mathbf{R}) = -\frac{dV(R-R_0)}{dR}\langle f; I_f M_f|\hat{\delta}_{\lambda\mu}|i; I_i M_i\rangle Y_{\lambda\mu}(\hat{R}) \tag{12}$$

The required structure input are the reduced matrix elements of the deformation operator which, in Reaction4Exp is given as a signed real number, the deformation length:

$$\langle f; KI_f\|\hat{\delta}_\lambda\|i; KI_i\rangle = \delta_\lambda \tag{13}$$

Note that, in the rotor model, the sign of δ_λ and $Mn(E\lambda)$ is the same. The Reaction4Exp calculations require the $Mn(E\lambda)$ and δ_λ parameters.

In general, both the Coulomb and nuclear interactions will contribute to the excitation and so the transition potential will be the sum of the nuclear and Coulomb transition potentials and, consequently, the corresponding scattering amplitude will be given by the coherent sum of the individual nuclear and Coulomb amplitudes, i.e.,

$$f_{if}(\theta) = f_{if}^N(\theta) + f_{if}^C(\theta). \tag{14}$$

Since the corresponding inelastic cross section is proportional to the square of $f_{if}(\theta)$, interference effects will occur between the nuclear and Coulomb parts.

It is common to use a dimensionless parameter, the deformation parameter β, to describe the deformation, which can be related to the inputs for the Reaction4Exp calculations through:

$$\beta_C = \frac{4\pi\langle I_i K\lambda 0|I_f K\rangle Mn(E\lambda)}{3ZeR_c^\lambda} \tag{15}$$

$$\beta_N = \frac{\delta_\lambda}{R_n}, \tag{16}$$

where Z is the charge of the deformed nucleus, R_c its average charge radius and R_n its average mass radius.

3 Reaction4Exp calculations

For the Reaction4Exp calculations, we will use the optical model potentials of Table I of Tenreiro *et al* (see Fig. 1). The considered excitation, $0^+ \to 2^+$ has necessarily $\lambda = 2$ so we will need the corresponding intrinsic reduced Coulomb matrix element and nuclear deformation length.

For the Coulomb part, we will consider a reduced Coulomb radius $r_C = 1.25$ fm and a value for $B(E2; gs; 0^+ \to 2^+)$, taken from experiment (Att. Nucl. Data Tables 80 p. 35 (2002)):

$$B(E2; gs; 0^+ \to 2^+) = 1680 \text{ e}^2\text{fm}^4.$$

For the nuclear part the reduced radius for the potential both for real and imaginary parts is $r_0 = 1.25$ fm.

Some important issues to take into account for a correct implementation of these calculations:

TABLE I. Summary of the potential parameters obtained from the optical model analysis of the elastic scattering angular distributions and deformation lengths βR obtained from the DWBA analysis, performed on the inelastic scattering angular distributions.

$E_{\text{c.m.}}$ (MeV)	V_0 (MeV)	a_v (fm)	W_0 (MeV)	a_w (fm)	$\beta_v R_v$ (fm)	$\beta_w R_w$ (fm)	χ^2
32.0	68.21	0.557	7.05	0.574	0.892	2.823	0.60
32.8	51.09	0.556	9.14	0.551	0.941	1.815	1.09
34.0	44.30	0.562	18.76	0.556	1.106	1.047	0.74
34.8	43.78	0.561	14.76	0.551	1.207	1.106	1.07
35.2	45.69	0.559	12.09	0.563	1.250	0.411	1.26
38.4	44.66	0.560	20.61	0.560	1.117	1.011	1.38
41.6	41.03	0.560	18.56	0.560	0.889	1.013	2.22
43.2	44.40	0.560	18.97	0.559	1.258	0.932	0.62
44.8	43.99	0.560	19.30	0.560	1.258	0.831	1.20
49.6	46.82	0.561	17.43	0.554	1.106	1.359	1.07
51.2	43.52	0.561	19.40	0.552	1.106	1.334	0.82

Figure 1: Optical model parameters from Tenreiro et el, PRC53, 2870 (1996).

- Table 1 presents the energy in the center of mass, but the input requires the energy in the laboratory frame, which is related to the center of mass one through $E_{\text{lab}} = E_{\text{cm}} \frac{A_t + A_p}{A_t}$
- The energy of the first 2^+ state of ^{64}Zn can be consulted in *https://www.nndc.bnl.gov/nudat3/*
- In this case the target is the one excited. As such the parameters for the deformation must be given for the target. As well, only the deformation for $\lambda = 2$ is relevant in this calculation.
- In Ref. I the authors use different deformations for the real and imaginary parts. Reaction4Exp has an option to provide these different values for the real and imaginary parts.
- A large value for the maximum total angular momentum $J_T > 100$ is required for convergence.

The results obtained for the elastic and inelastic cross sections are displayed in Fig. 2.

It is illustrative to study the separate effect of the Coulomb and nuclear couplings in the inelastic cross sections. For this purpose, we can set to zero the corresponding input in the calculation. The results are also included in Fig. 2. From these curves, several conclusions can be drawn:

- The Coulomb excitation mechanism is dominant at the smaller scattering angles, whereas the nuclear excitation dominates the larger scattering angles. This is a direct consequence of the "long-range" versus "short-range" nature of these interactions.
- Around $\theta_{\text{c.m.}} \approx 100^\circ$ the Coulomb and nuclear cross sections are of similar magnitude, and hence the interference effect between both contributions is apparent at these angles. Moreover, we see that this interference is of destructive nature.

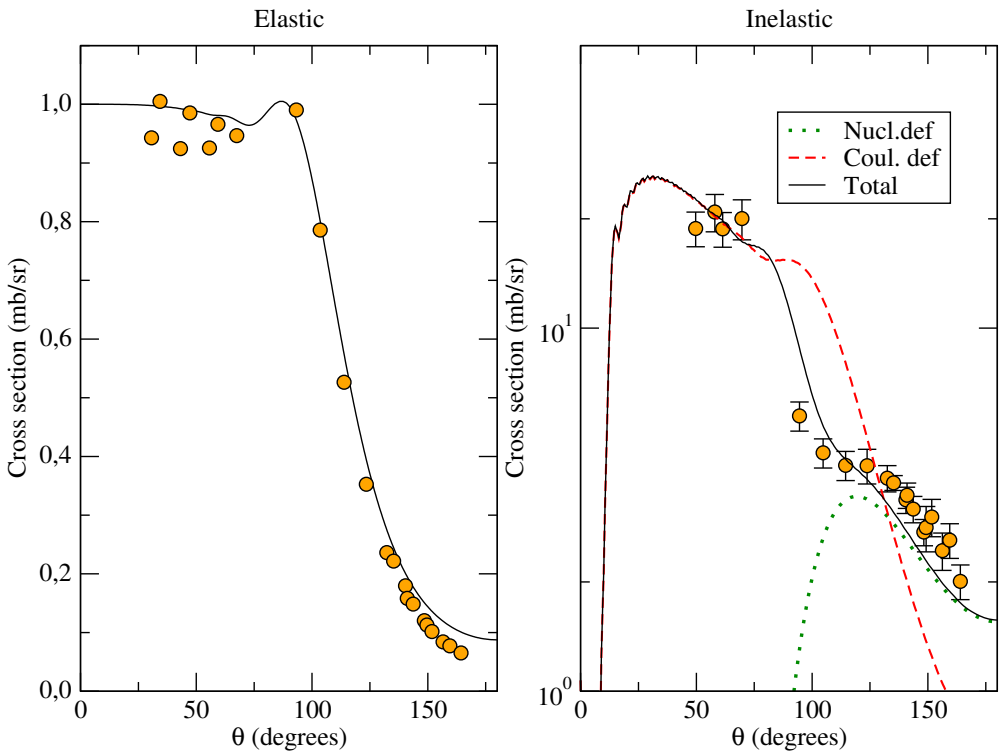

Figure 2: Left: Elastic differential cross section (relative to Rutherford cross section) for $E_{\text{c.m.}} = 35,2$ MeV. Right: inelastic differential cross section.